Simulation of inter atrial block based on a human atrial model

Gao, Y., Gong, Y. L., Xia, L. & Zheng, D. C.

Original citation & hyperlink:
Gao, Y, Gong, YL, Xia, L & Zheng, DC 2019, 'Simulation of inter atrial block based on a human atrial model' Journal of Zhejiang University: Science A, vol. 20, no. 4, pp. 300-309. https://dx.doi.org/10.1631/jzus.B1800420

DOI 10.1631/jzus.B1800420
ISSN 1673-1581
ESSN 1862-1783

Publisher: Springer

The final publication is available at Springer via http://dx.doi.org/10.1631/jzus.B1800420

Simulation of inter atrial block based on a human atrial model

Yuan GAO[1†], Ying-lan GONG[1†], Ling XIA[1*], Ding-chang ZHENG[2]

[1] Key Laboratory for Biomedical Engineering of Ministry of Education, *Department of Biomedical Engineering, Zhejiang University, Hangzhou 310027, China*

[2]*Health and Wellbeing Academy, Faculty of Medical Science, Anglia Ruskin University, Chelmsford, CM1 1SQ, UK*

[†]: co-first author. [*]: E-mail: xialing@zju.edu.cn

Abstract

Inter atrial block (IAB) is a prevailing cardiac conduction abnormality that is under-recognized in clinical practice. IAB has strong association with atrial arrhythmia, left atrial enlargement, and electromechanical discordance, increasing the risk of atrial fibrillation (AF) and myocardial ischemia. IAB was generally believed to be caused by impaired conduction along Bachmann bundle (BB). However, there are three other conduction pathways, including the posteriorly in the vicinity of the right pulmonary veins (VRPV), transseptal fibers in the fossa ovalis (FO) and muscular bundles on the inferior atrial surface near the coronary sinus (CS). We hypothesized that the importance of BB on IAB might have been overestimated. To test this hypothesis, various combinations conduction pathways block were simulated based on a realistic human atrial model to investigate their effects on the index of clinical diagnosis standard of IAB using simulated 12-lead electrocardiogram (ECG). The results showed that the BB block alone could not generate typical P wave morphology of IAB, and that the combination of BB and VRPV pathways block played important roles in the occurrence of IAB. Secondly, although single FO and CS pathway play subordinate roles in the inter atrial conduction, their combination with BB and VRPV block could also produce severe IAB. In summary, this simulation study has demonstrated that the combinations of different inter atrial conduction pathways, rather than BB alone, resulted in ECG morphology of IAB, which needs to be paid attention in the future pathophysiological and clinical studies of IAB.

1 Introduction

Inter atrial block (IAB) is defined as prolonged conduction time between the right and left atrium due to impulse delay or blockage, leading to prolonged P-wave duration (>120 ms) on surface electrocardiogram (ECG) (Tse *et al.*, 2017). IAB can be graded as partial and advanced, depending on the severity of the conduction delay (Bayés *et al.*, 2012, Kitkungvan and Spodick, 2009). Partial IAB is characterized by bifid morphology of ECG P waves on leads I, II, III and

aVF. While advanced IAB is characterized by biphasic P waves on lead V1 and inferior leads (II, III and aVF) (Martínez‐Sellés *et al.*, 2017, Tse *et al.*, 2016). IAB was first described experimentally by Bachmann in 1916 (Bachmann, 1916). But unlike other common cardiac diseases, IAB is still poorly perceived and underappreciated in clinical practice, despite its high prevalence in inpatient and outpatient populations (Lovely *et al.*, 2014, Spodick and Ariyarajah, 2010).

The prevalence of IAB is age dependent, increasing from about 5% for individuals less than 20 years old to 60% at ages over 50 years (Gialafos *et al.*, 2007, Martínezsellés *et al.*, 2016). IAB can lead to delayed and asynchronous activation of the left atrium, increasing the risks of atrial arrhythmias and ischemic stroke (Ariyarajah *et al.*, 2007, He *et al.*, 2017), left atrial enlargement, left atrial electromechanical dysfunction, and thromboembolism (Wu *et al.*, 2017). Previous studies have implicated that IAB is a potential risk factor of atrial fibrillation (AF) (Bayés *et al.*, 2017, Massó-Van *et al.*, 2017), the presence of IAB was shown to be related to the development of new onset and recurrence of AF (Alexander *et al.*, 2017, Enriquez *et al.*, 2015, Fernándezfernández, 2017, Tekkesin *et al.*, 2017). Moreover, IAB is associated with the deterioration of paroxysmal AF into chronic and permanent forms of AF (Abe *et al.*, 1997).

However, the underlying mechanism directly affecting IAB has not been fully elucidated. Coronary artery disease and other common cardiovascular risk factors, such as diabetes mellitus, hypertension, hypercholesterolemia, obesity, smoking and physical inactivity, have been proposed to be the pathogenesis of IAB (Ariyarajah and Spodick, 2006, Vignendra *et al.*, 2007). IAB is generally considered to be caused by impaired conduction along Bachmann bundle (BB) (O'Neal *et al.*, 2016, Tse, Lai, Jie and Yan, 2016). But there are three other conduction pathways, including the posteriorly in the vicinity of the right pulmonary veins (VRPV), transseptal fibers in the fossa ovalis (FO) and muscular bundles on the inferior atrial surface near the coronary sinus (CS). Tapanainen et al studied the conduction pathway in patients with paroxysmal AF, where concluded that BB might not exclusively serve as the preferential or dominant route for inter atrial conduction (Tapanainen and Jurkko, 2009). This implies that the importance of BB in IAB may be overestimated.

The main aim of this study was to investigate the combinational effects of the four inter atrial pathway blocks on the occurrence of IAB. To achieve the objectives, various combinations of conduction pathway blocks would be simulated based on a realistic human atrial model, and the

simulated 12-lead ECG would be used to test their effect on the index of standard clinical diagnosis of IAB.

2 Material and methods

2.1 Anatomical model

The atrial model was constructed based on healthy adult male heart specimen obtained from Zhujiang Hospital, Southern Medical University, China. The Chinese Law on Heart Research using heart specimen has been strictly followed. The specimen was scanned using a spiral computerized tomography (Philips / Brilliance 64) with a resolution of 512×512 pixel and the spatial resolution was 0.3574 mm×0.3574 mm×0.33 mm (Fig. 1). The details of the model can be found in our previous study (Deng *et al.*, 2012, Deng *et al.*, 2012, Gong *et al.*, 2015).

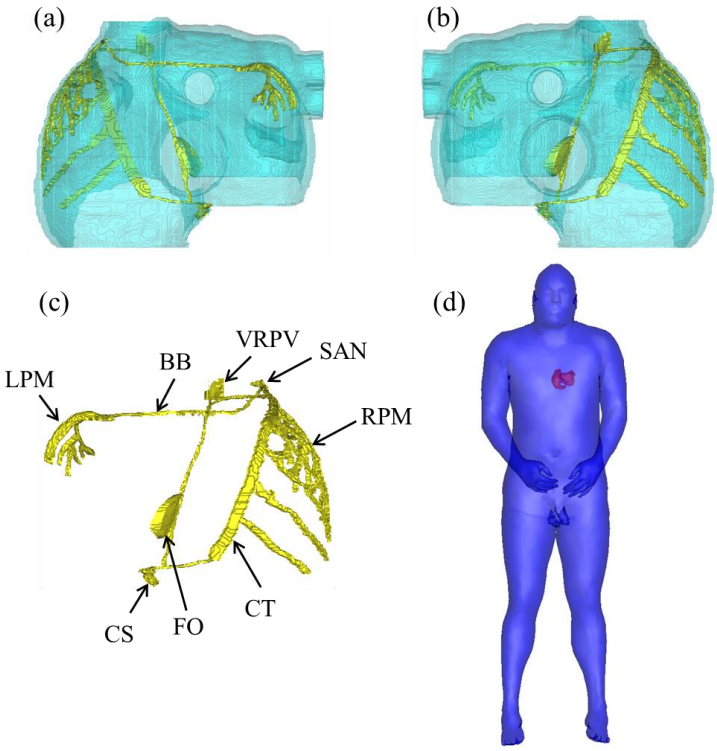

Figure 1 Illustration of the atrium and torso model: (a) anterior view of atrium; (b) posterior view of atrium. The cyan color indicates atrial muscles, and the yellow color indicates conduction system; (c) conduction system; (d) the merge of the atrium into the body. SAN: sinus node; CT: crista terminalis; BB: Bachmann bundle; VRPV: vicinity of the right pulmonary veins; FO: fossa ovalis; CS: coronary sinus; LPM: left atrium pectinate muscle; RPM: right atrium pectinate muscle.

The conduction system in the constructed model consisted of sinus node (SAN), crista terminalis (CT), pectinate muscles (PM) and inter atrial impulse propagation routes. The inter

atrial conduction pathway included BB, VRPV, FO, and CS. The atrial fiber orientation was contained to simulate the anisotropy. The atrial cell in this study was based on the model developed by Courtemanche et al. (Courtemanche *et al.*, 1998). During the activation propagation, each myocardial unit has specific electrophysiological parameters associated with the action potential (AP) of the cell unit and conduction velocity.

2.2 Numerical method

The excitation conduction was simulated based on the monodomain equation (Zhang *et al.*, 2007):

$$\frac{\partial V_{\mathrm{m}}}{\partial t}=\frac{1}{C_{\mathrm{m}}}\left(\frac{1}{A_{\mathrm{m}}}\left(\frac{\lambda}{1+\lambda}\nabla\cdot\left(\sigma_{\mathrm{i}}\nabla V_{\mathrm{m}}\right)-I_{\mathrm{ion}}+I_{\mathrm{app}}\right)\right), \tag{1}$$

where V_{m} is transmembrane voltage, t is time, C_{m} is the membrane capacitance, A_{m} is surface to volume ratio, λ is the ratio of conductivity extracellular to intracellular, σ_{i} is cellular conductivity, I_{ion} is the sum of ionic currents, I_{app} is the sum of applied stimulus currents.

Equation (1) was solved numerically by using explicit Euler method based on parallel computational techniques. The simulation was computed on a cluster of networked Dawning TC4000L system. It had multiple symmetrical parallel processors that contained a management node and ten computation nodes. Each computation node consisted of two Intel Xeon 5335 processors (each 4-core) and 4GB memory. The total theoretical computing capacity was up to 184Gflops. MPICH2 was used to implement the communication between nodes.

In this study, the torso model was taken from the virtual male subject of the United States (Ackerman, 1991). The body surface potentials generated by the cardiac sources satisfy the Poisson equation with Newman boundary conditions:

$$\begin{cases}\nabla\cdot(\sigma\nabla\Phi)=-\nabla\cdot\boldsymbol{J}_{\mathrm{s}}, & \text{in } \Omega\\ \sigma(\nabla\Phi)\cdot\boldsymbol{n}=0, & \text{on } S_{\mathrm{B}}\end{cases}, \tag{2}$$

where σ is tissue dependent conductivity tensor, Φ is quasi static potential, $\boldsymbol{J}_{\mathrm{s}}$ is the density of the equivalent dipole sources, $\boldsymbol{n}$ is normal vector, S_{B} is the body surface, which encloses the volume conductor Ω.

Using the Green second identity:

$$\int_S\left(A\nabla B-B\nabla A\right)\cdot\boldsymbol{n}\,\mathrm{d}S=\int_V\left(A\nabla^2B-B\nabla^2A\right)\mathrm{d}\Omega \tag{3}$$

with $A=\frac{1}{R}$ ($R=\left|\boldsymbol{r}-\boldsymbol{r}_{\mathrm{s}}\right|$ is the distance between the field point $\boldsymbol{r}$ and source point $\boldsymbol{r}_{\mathrm{s}}$) and $B=\sigma\Phi$,

the differential equation for Φ as (5) can be solved as follows:

$$\Phi(\boldsymbol{r}) = \frac{1}{4\pi\sigma}\left(\int_{\Omega_h} \boldsymbol{J}_s \cdot \nabla \frac{1}{R} \mathrm{d}V + \sum_{l=1}^{m} \left(\sigma_l^+ - \sigma_l^-\right) \int_{S_l} \Phi(\boldsymbol{r}) \nabla \frac{1}{R} \mathrm{d}S\right) \tag{4}$$

where Ω_h is the heart area, S_l (l=1,2,…,m) is the conductivity junction surface, and its inside and outside conductivities are σ_l^- and σ_l^+ , respectively. Further details of the model were described in our previous studies (Shou *et al.*, 2007, Xia *et al.*, 2006).

The 12-leads ECGs are calculated as (Kligfield *et al.*, 2007)

$$\begin{aligned}
\mathrm{I} &= V_{\mathrm{LA}} - V_{\mathrm{RA}} \\
\mathrm{II} &= V_{\mathrm{LL}} - V_{\mathrm{RA}} \\
\mathrm{III} &= V_{\mathrm{LL}} - V_{\mathrm{LA}} \\
\mathrm{aVR} &= -\frac{1}{2}\left(\mathrm{I} + \mathrm{II}\right) \\
\mathrm{aVL} &= \mathrm{I} - \frac{1}{2}\mathrm{II} \\
\mathrm{aVF} &= \mathrm{II} - \frac{1}{2}\mathrm{I} \\
\mathrm{V}_i &= V_{\mathrm{P}i} - \left(V_{\mathrm{LA}} + V_{\mathrm{RA}} + V_{\mathrm{LL}}\right) / 3
\end{aligned} \tag{5}$$

where V_{LA} is left arm surface potential, V_{RA} is right arm surface potential, V_{LL} is left leg surface potential, V_i is each precordial lead (i=1,2…6), V_{Pi} is each precordial surface potential.

3 Results

3.1 One conduction pathway block alone

Figure 2 shows the exciting sequence maps of atrium with one conduction pathway block alone. For comparison, the normal atrial exciting sequence maps were also presented on the top of Figure 2. The normal depolarization duration of right atrium was 86 ms. The initial onset of LA activation through the BB conduction pathway was located at anterior wall near the left atrial appendage at 37 ms. The total depolarization time of atrium was 103 ms at the area of posterior left atrial wall.

With the conduction pathway block of BB only, the activation wave has to pass through the other three pathways from the atrial septum. This extended the propagation distance and prolonged the total depolarization time of atrium to 113 ms.

With the conduction pathway block of VRPV only, since the BB pathway was in normal condition, the exciting sequence of LA anterior wall had no obvious change, but the activation wave from RA posterior wall to LA posterior wall was apparently separated. The activation wave had to pass through the BB and propagated cross the roof of LA to converge with the wave that

passed through the FO pathway. This changed the exciting sequence of LA posterior wall but the propagation direction was still forward and the total depolarization time was only prolonged to 104 ms.

With the conduction pathway block of FO only, the activation wave passed through VRPV pathway and propagated to the area that should have been activated by the FO pathway, so the atrial exciting sequence maps were similar to the normal case. The total depolarization time of atrium was 105 ms. Finally, with the block of SC only, the activation wave could pass through FO and propagated to the area that should have been activated by the CS pathway, so the atrial exciting sequence maps had no change in comparison with the normal case and the total depolarization time of atrium was also 103 ms.

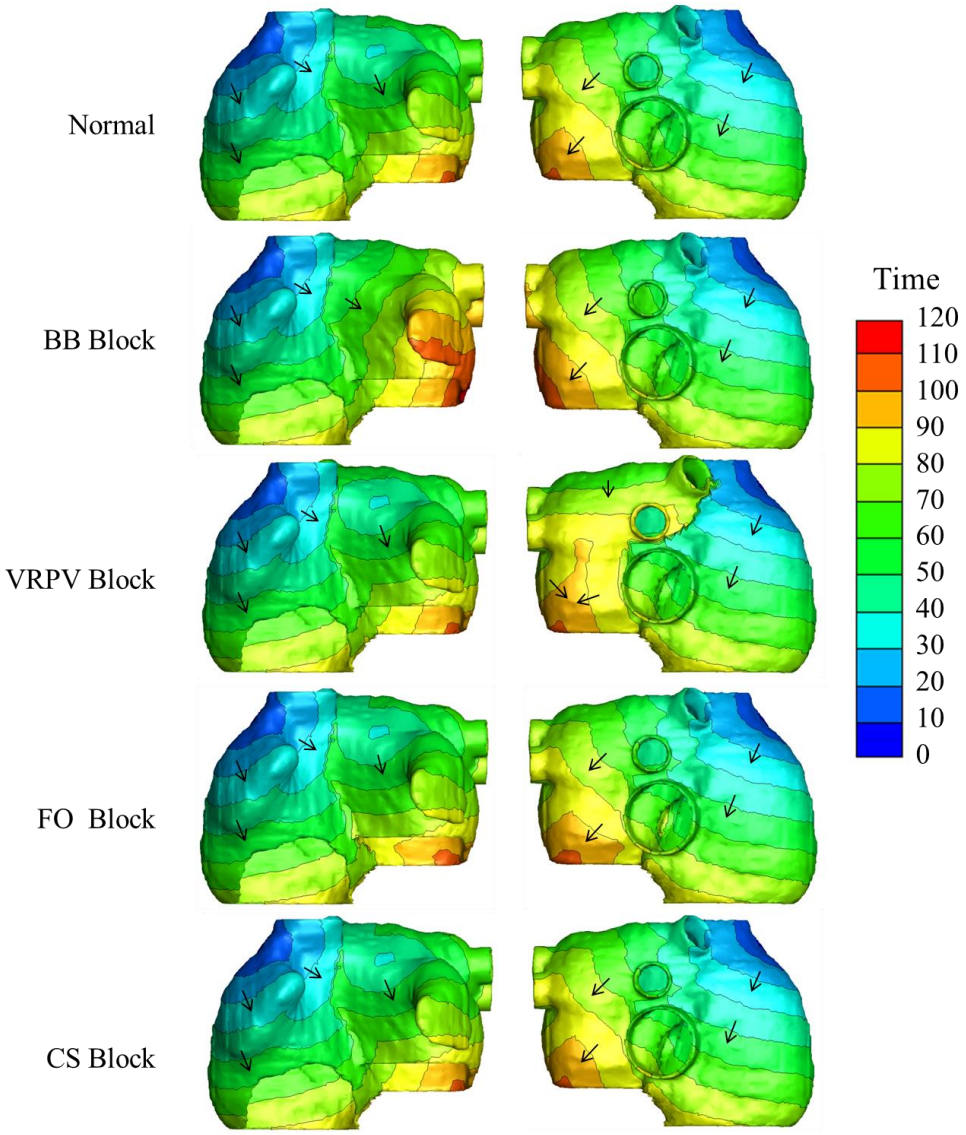

Figure 2 Simulated activation sequences with one conduction pathway block alone (from top to the bottom: normal

atrium; then with BB, VRPV, FO and CS block). The arrows indicate the wave propagation direction. The color bar on the right-hand side indicates the propagation time with the units in milliseconds.

Figure 3 and Figure 4 show the P wave of the simulated 12 lead ECG of atrium with one conduction block in comparing with normal atrium. When BB conduction pathway alone was blocked, the atrial total depolarization time was obviously prolonged, leading the ECG P wave duration up to 113 ms, but this did not reach the IAB criteria (P wave duration >120 ms). Likewise, the morphology of P wave was still positive. This is because the VRPV conduction pathway was in normal condition, so the activation wave still could propagate from the superior of LA.

When the VRPV conduction pathway was blocked alone, the exciting sequence of atrial posterior wall was changed, but the propagation direction was still forward, resulting in that there was no obvious difference in P wave in comparison with the normal case. As shown in Figure 4, when the FO or CS conduction pathway was blocked alone, the atrial exciting sequence barely changed, and the P wave was nearly the same as normal case.

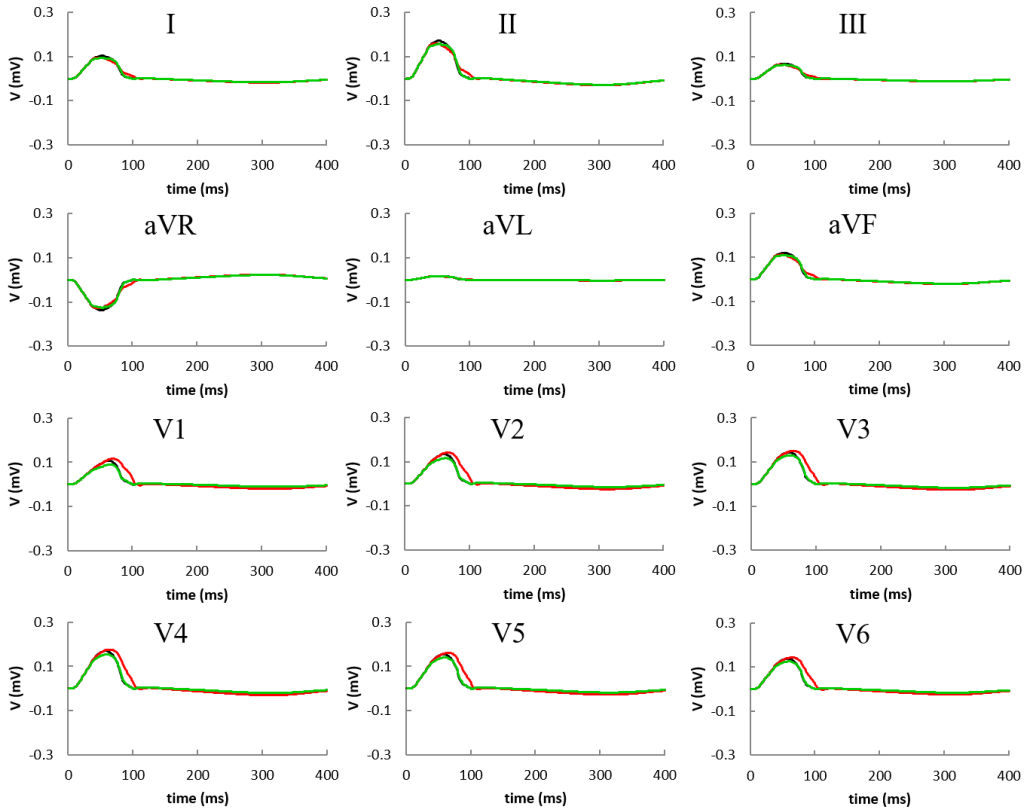

Figure 3 Simulated P wave of 12 lead ECG with one conduction pathway block alone. The black lines are from the normal cases, red lines are with BB block, and green lines are with VRPV block.

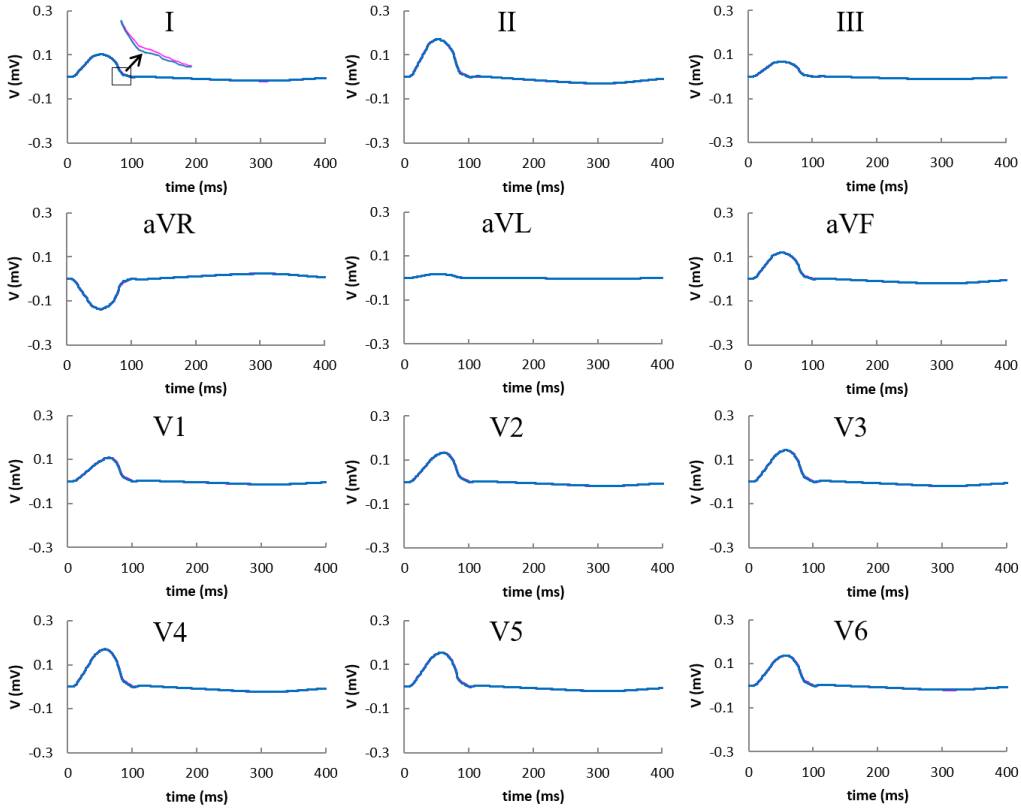

Figure 4 Simulated P wave of 12 lead ECG with one conduction pathway (FO or CS) block alone. The black lines are the normal case, pick lines are with FO block, blue lines are with CS block. As the FO and CS block were similar to normal case, the lines were overlapped. On lead I, a local enlarged window is given to illustrate the minor differences.

3.2 Two conduction pathways block

Figure 5 showed exciting sequence maps of atrium with the block form two conduction pathways. When the two superior pathways (BB and VRPV) were both blocked, the activation wave could only pass through inferior pathways (FO and CS). This led to the retrograde activation of LA in the caudo-cranial direction. The total depolarization time of atrium was prolonged to 124 ms. With the block of BB+FO or BB+CS, the activation wave could pass through the normal VRPV and the wave still propagated in forward direction,. The total depolarization time of atrium was 114 and 113 ms, respectively.

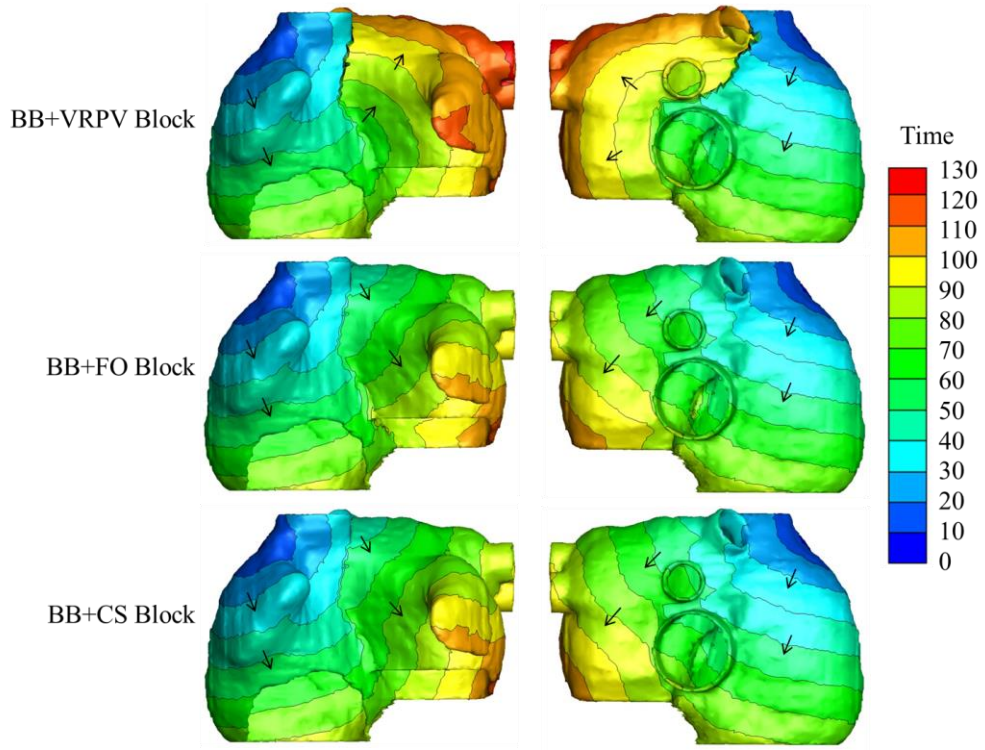

Figure 5 Simulated activation sequences with the block of two conduction pathways (from the top to bottom: BB and VRPV block; BB and FO block; BB and CS block). The arrows indicate the wave propagation direction. The color bar on the right-hand side indicates the propagation time with the units in milliseconds.

Figure 6 shows the simulated P wave of the 12 lead ECG of atrium with two conduction block. When BB and VRPV conduction pathways were blocked, the retrograde activation of LA resulted in biphasic P waves in lead V1 and the inferior leads (II, III and aVF), leading to prolonged P wave duration of 124 ms. Both the P wave morphology and duration time satisfied the diagnostic criteria of IAB. When the conduction pathways of BB+FO or BB+CS were blocked, the simulated morphology of P wave was still positive.

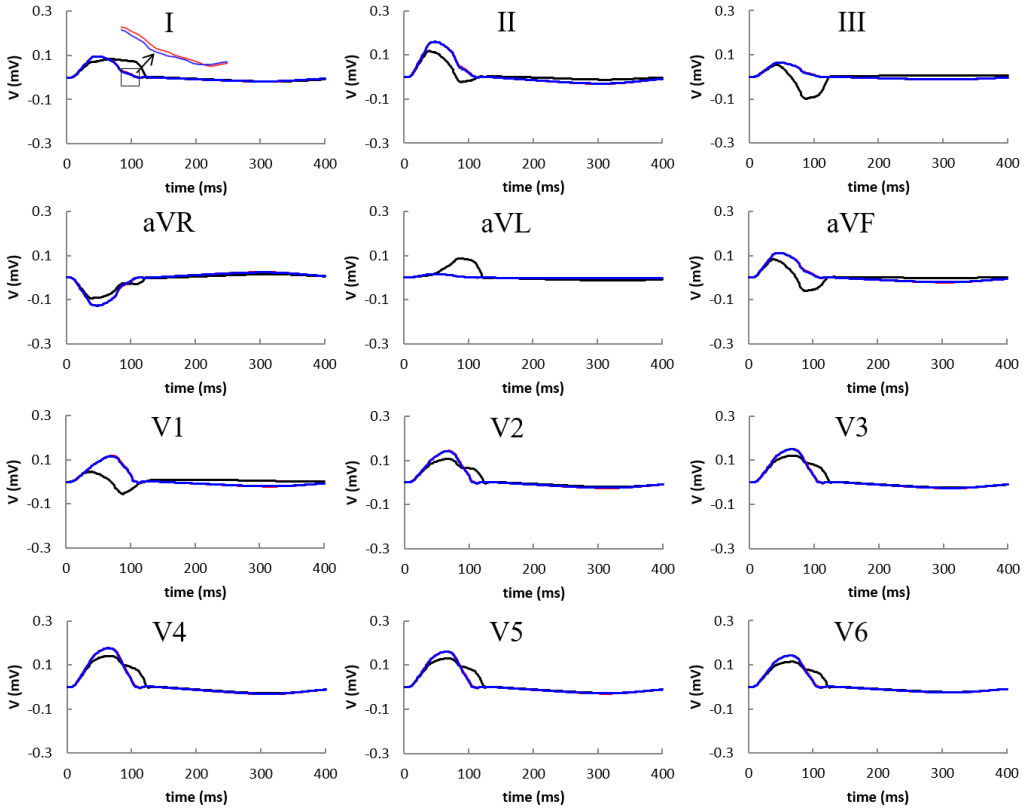

Figure 6 Simulated P wave of 12 lead ECG with the block of two conduction pathways (BB+VRPV or BB+FO or BB+CS). The black lines are with BB and VRPV block, red lines are with BB and FO block, and blue lines are with BB and CS block. As red and blue lines were overlapped since their simulated results were the very similar.

3.3 Three conduction pathways block

Figure 7 shows the exciting sequence maps of atrium with the block of three conduction pathways. When the BB, VRPV and FO were blocked, the activation wave had to propagate to CS pathway first, and then retrograded to LA, leading to propagation distance and resulting in the significantly prolonged depolarization time of atrium of 160 ms. Similarly, with the block of BB, VRPV and CS, the activation wave had to pass through FO pathway first, and then retrograded to LA. While the propagation speed at FO is superior to CS pathway, the depolarization time of atrium was only prolonged to 124 ms.

Figure 8 shows the simulated P wave of the 12 lead ECG of atrium with the block of three conduction pathways. The block of BB+VRPV+FO or BB+VRPV+CS both produced significant biphasic P waves in lead V1 and the inferior leads.

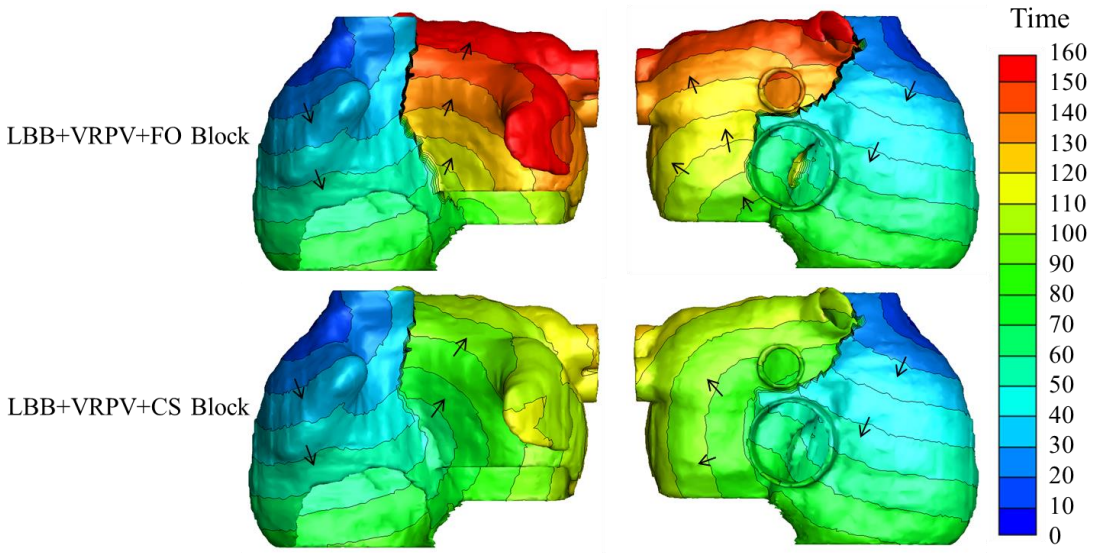

Figure 7 Simulated activation sequences with three conduction pathways block. Top: BB, VRPV and FO block; Bottom: BB, VRPV and CS block. The arrows indicate the wave propagation direction. The color bar on the right-hand side indicates the propagation time with the units in milliseconds.

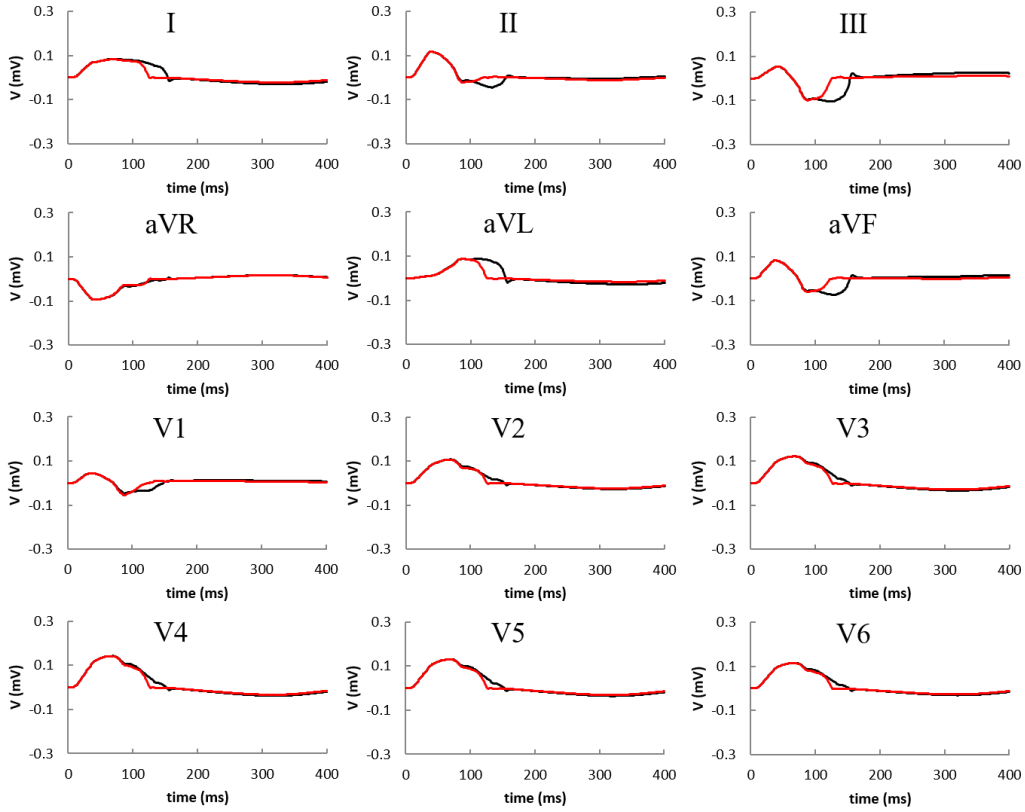

Figure 8 12 lead ECG with three conduction pathway block. The black lines are BB, VRPV and FO block, red lines are BB, VRPV and CS block.

Table 1 gives a summary of P wave duration and morphology with different combinations of

conduction pathway block. It can be seen that, to achieve the criteria of IAB, the combinational block of BB and VRPV was required.

Table 1 Summary of P wave duration and morphology with different combinations of conduction pathway block.

Cases	P wave duration (ms)	P wave morphology
Normal	103	Positive
BB Block	113	Positive
VRPV Block	104	Positive
FO Block	105	Positive
CS Block	103	Positive
BB+VRPV Block	**124**	**Biphasic**
BB+FO Block	114	Positive
BB+CS Block	113	Positive
BB+VRPV+FO Block	**160**	**Biphasic**
BB+VRPV+CS Block	**124**	**Biphasic**

4 Discussions

This study investigated the effects of IAB with various conduction pathways block combinations. The simulation results indicated that the block of BB only could increase the P wave duration by 10 ms, but the morphology and polarity remained nomral. With the block of the other three conduction pathways (VRPV, FO or CS), no obvious change in P wave duration and morphology was observed. The simulation results were in accordance with reported data from canine experiments (Waldo *et al.*, 1971), indicating that single pathway block could not make P wave morphology satisfy the typical diagnostic criteria of IAB. The results also showed that when VRPV pathway was in normal condition, the FO or CS pathway block has minor influence on the atrial activation sequence and P wave morphology. So the importance of the four conduction pathway follows as BB, VRPV, FO and CS (i.e. the superior pathway was more important than the inferior pathway).

This study also simulated the effect of blocking two conduction pathways. When BB and VRPV were both blocked, the activation wave could only pass through inferior pathways. This

result in the retrograde activation of LA in the caudo-cranial direction, leading to biphasic P waves in lead V1 and the inferior leads (II, III and aVF). The morphology and duration time all satisfied the diagnostic criteria of IAB. The other two cases (BB and FO block; BB and CS block), due to the VRPV pathway was in normal condition, the activation sequence of LA was still in forward direction. So the P wave duration increased but morphology remained the same. These results indicated that retrograde activation of LA in the caudo-cranial direction was the substantial reason of P wave polarity change, so both BB and VRPV pathways play the important roles in IAB.

The final finding from this study was that, when BB, VRPV and FO were blocked, the retrograde activation of LA has the maximum propagation distance, leading to the longest P wave duration and significant biphasic P waves in lead V1 and the inferior leads. When BB, VRPV and CS were blocked, due to FO pathway was superior to CS pathway, the P wave duration was shorter and also have biphasic P waves in lead V1 and the inferior leads. This indicated that although single inferior pathway play subordinate role in the inter-atrial conduction, their combination with other pathway could produce more severe IAB.

At present, clinical treatment of IAB has not yet reached a unified understanding. The study of biatrial pacing and right atrial appendage pacing on IAB showed that biatrial pacing could effectively reduce the concentrations of atrial natriuretic peptide (ANP) and markers of inflammation (high sensitivity C-reactive protein (hs-CRP), interleukin 6 (IL-6) , and neopterin), indicating biatrial pacing improves hemodynamic performance in patients with IAB and preserved atrio-ventricular conduction (Rubaj *et al.*, 2013). Burri et al. also showed that biatrial pacing in comparison to pacing from interatrial septum or coronary sinus or right atrial appendage could result in favorable acute atrial hemodynamic and atrioventricular synchrony (Burri *et al.*, 2011). The conclusions confirmed our simulation results, indicating that IAB is not caused by single pathway block along.

The studies of patients with sinus node dysfunction and intra atrial conduction delay showed that low interatrial septum pacing could reduce P wave duration and prevent the development of persistent AF (Lau *et al.*, 2013, Verlato *et al.*, 2011). This is consistent with our simulation results of multichannel block, confirming that the role of inferior pathways can not be ignored in IAB.

At present, the biatrial pacing, atrial septum pacing and Bachmann pacing all showed efficacy for the prevention of the occurrence of IAB. However, the sample size of each study is small and conclusion is varied. Therefore, these atrial pacing methods are currently not clinically

recommended for the treatment of IAB. Our simulation results have a guiding role in explaining the mechanism of IAB and confirming the effect of pacing therapy and the placement of pacemakers. Moreover, according to the clinical diagnostic criteria of IAB the lower limit of P wave duration of IAB has to be more than 120ms, our simulation showed that the P wave duration was varied with different pathways block, indicating P wave duration values may be used as an underlying tool to identify various combinations of pathways block.

It should be pointed out that there is limitation in the present study. The model used in our simulation was a static heart model with electrophysiological properties. The mechanical functions of the heart have not been involved. Cardiac motion should take into consideration in future studies to improve the simulation accuracy.

5 Conclusions

In summary, this simulation study has demonstrated that at least the combinational block of BB and VRPV is required to have the P wave duration and morphology to meet the typical diagnostic criteria of IAB, providing better understanding of underlying mechanism of IAB and some guidelines for future pathophysiological and clinical studies of IAB.

Acknowledgement

This work was supported by the National R&D Program for Major Research Instruments (grant no. 61527811), the National Natural Science Foundation of China (grant no. 61701435), and the Zhejiang Provincial Natural Science Foundation of China (LY17H180003).

Compliance with ethics guidelines

Yuan GAO, Ling XIA, Ying-lan GONG, and Ding-chang ZHENG declare that they have no conflict of interest.

All procedures followed were in accordance with the ethical standards of the responsible committee on human experimentation (institutional and national) and with the Helsinki Declaration of 1975, as revised in 2008 (5). Informed consent was obtained from all patients for being included in the study.

References

Abe, Y., Fukunami, M., Yamada, T., Ohmori, M., Shimonagata, T., Kumagai, K., *et al.*, 1997. Prediction of transition to chronic atrial fibrillation in patients with paroxysmal atrial fibrillation by signal-averaged electrocardiography: a prospective study. *Circulation*, **96**(8):2612. [doi: 10.1161/01.CIR.96.8.2612]

Ackerman, M.I., 1991. Viewpoint : The visible human project. *J. Biocommun*, **18**(2):14.

Alexander, B., Machaalany, J., Lam, B., Rooy, H.V., Haseeb, S., Kuchtaruk, A., *et al.*, 2017. Comparison of the Extent of Coronary Artery Disease in Patients With Versus Without Interatrial Block and Implications for New-Onset Atrial Fibrillation. *American Journal of Cardiology*, **119**(8):1162. [doi: 10.1016/j.amjcard.2016.12.032]

Ariyarajah, V., Apiyasawat, S., Najjar, H., Mercado, K., Puri, P. and Spodick, D.H., 2007. Frequency of interatrial block in patients with sinus rhythm hospitalized for stroke and comparison to those without interatrial block. *American Journal of Cardiology*, **99**(1):49-52. [doi: 10.1016/j.amjcard.2006.07.060]

Ariyarajah, V. and Spodick, D.H., 2006. The Bachmann Bundle and interatrial conduction. *Cardiology in Review*, **14**(4):194.

Bachmann, G., 1916. THE INTER-AURICULAR TIME INTERVAL. *Arquivos Brasileiros De Endocrinologia E Metabologia*, **55**(6):357-8. [doi: 10.1152/ajplegacy.1916.41.3.309]

Bayés, d.L.A., Martínez-Sellés, M., Bayés-Genís, A., Elosua, R. and Baranchuk, A., 2017. Surface ECG interatrial block-guided treatment for stroke prevention: rationale for an attractive hypothesis. *Bmc Cardiovascular Disorders*, **17**(1):211. [doi: 10.1186/s12872-017-0650-y]

Bayés, d.L.A., Platonov, P., Cosio, F.G., Cygankiewicz, I., Pastore, C., Baranowski, R., *et al.*, 2012. Interatrial blocks. A separate entity from left atrial enlargement: a consensus report. *Journal of Electrocardiology*, **45**(5):445-451. [doi: 10.1016/j.jelectrocard.2012.06.029]

Burri, H., Bennani, I., Domenichini, G., Garnière, V., Sunthorn, H., Stettler, C., *et al.*, 2011. Biatrial pacing improves atrial haemodynamics and atrioventricular timing compared with pacing from the right atrial appendage. *Europace : European pacing, arrhythmias, and cardiac electrophysiology : journal of the working groups on cardiac pacing, arrhythmias, and cardiac cellular electrophysiology of the European Society of Cardiology*, **13**(9):1262-1267(6). [doi: 10.1093/europace/eur099]

Courtemanche, M., Ramirez, R.J. and Nattel, S., 1998. Ionic mechanisms underlying human atrial action potential properties: insights from a mathematical model. *American Journal of Physiology*, **275**(1 Pt 2):H301-21.

Deng, D., Jiao, P., Ye, X. and Ling, X., 2012. An Image-Based Model of the Whole Human Heart with Detailed Anatomical Structure and Fiber Orientation. *Computational & Mathematical Methods in Medicine*, **2012**(3):449-461. [doi: 10.1155/2012/891070]

Deng, D.D., Gong, Y.L., Shou, G.F., Jiao, P.F., Zhang, H.G., Ye, X.S., *et al.*, 2012. Simulation of biatrial conduction via different pathways during sinus rhythm with a detailed human atrial model. *Journal of Zhejiang University-SCIENCE B*, **13**(9):676-694. [doi: 10.1631/jzus.B1100339]

Enriquez, A., Sarrias, A., Villuendas, R., Ali, F.S., Conde, D., Hopman, W.M., *et al.*, 2015. New-onset atrial fibrillation after cavotricuspid isthmus ablation: identification of advanced interatrial block is key. *Europace*, **17**(8):1289. [doi: 10.1093/europace/euu379]

Fernándezfernández, F.J., 2017. Atrial Fibrillation: Interatrial Block May Be an Underdiagnosed and Easily Recognizable Risk Factor. *Mayo Clinic Proceedings*. [doi: 10.1016/j.mayocp.2017.01.022]

Gialafos, E., Psaltopoulou, T., Papaioannou, T.G., Synetos, A., Dilaveris, P., Andrikopoulos, G., *et al.*, 2007. Prevalence of interatrial block in young healthy men<35 years of age. *American Journal of*

Cardiology, **100**(6):995-997. [doi: 10.1016/j.amjcard.2007.04.041]

Gong, Y., Gao, Y., Lu, Z., Zheng, D., Deng, D. and Xia, L., 2015. Preliminary Simulation Study of Atrial Fibrillation Treatment Procedure Based on A Detailed Human Atrial Model. *Journal of Clinical Trials in Cardiology*, **2**(4):1-9. [doi: 10.15226/2374-6882/2/4/00130]

He, J., Tse, G., Korantzopoulos, P., Letsas, K.P., Ali-Hasan-Al-Saegh, S., Kamel, H., *et al.*, 2017. P-Wave Indices and Risk of Ischemic Stroke: A Systematic Review and Meta-Analysis. *Stroke*, **48**(8):2066. [doi: 10.1161/STROKEAHA.117.017293]

Kitkungvan, D. and Spodick, D.H., 2009. Interatrial block: is it time for more attention? *Journal of Electrocardiology*, **42**(6):687-692. [doi: 10.1016/j.jelectrocard.2009.07.016]

Kligfield, P., Gettes, L.S., Bailey, J.J., Childers, R., Deal, B.J., Hancock, E.W., *et al.*, 2007. Recommendations for the Standardization and Interpretation of the Electrocardiogram. *Journal of the American College of Cardiology*, **49**(10):1109-1127. [doi: 10.1016/j.jacc.2007.01.024]

Lau, C.P., Tachapong, N., Wang, C.C., Wang, J.F., Abe, H., Kong, C.W., *et al.*, 2013. Prospective randomized study to assess the efficacy of site and rate of atrial pacing on long-term progression of atrial fibrillation in sick sinus syndrome: Septal Pacing for Atrial Fibrillation Suppression Evaluation (SAFE) Study. *Circulation*, **128**(7):687-693. [doi: 10.1161/CIRCULATIONAHA.113.001644]

Lovely, C., Ramprakash, D., Chaubey, V.K. and Spodick, D.H., 2014. Interatrial Block in the Modern Era. *Current Cardiology Reviews*, **10**(3):181-189. [doi: 10.2174/1573403X10666140514101748]

Martínez-Sellés, M., Baranchuk, A., Elosua, R. and De Luna, A.B., 2017. Rationale and design of the BAYES (Interatrial Block and Yearly Events) registry. *Clinical Cardiology*, **40**([doi: 10.1002/clc.22647]

Martínezsellés, M., Roessel, A.M., J, Á., Bg, D.L.V., Cruzjentoft, A.J., Vidán, M.T., *et al.*, 2016. Interatrial Block and Atrial Arrhythmias in Centenarians: Prevalence, Associations, and Clinical Implications. *Heart Rhythm*, **13**(3):645-651. [doi: 10.1016/j.hrthm.2015.10.034]

Massó-Van, R.A., Escobar-Robledo, L.A., I, R.D., Grau, M., Sala, J., Ramos, R., *et al.*, 2017. Analysis of the Association Between Electrocardiographic P-wave Characteristics and Atrial Fibrillation in the REGICOR Study. *Revista Espanola De Cardiologia*. [doi: 10.1016/j.rec.2017.02.019]

O'Neal, W.T., Zhang, Z.M., Loehr, L.R., Chen, L.Y., Alonso, A. and Soliman, E.Z., 2016. Electrocardiographic Advanced Inter-Atrial Block and Atrial Fibrillation Risk in the General Population. *American Journal of Cardiology*, **117**(11):1755-1759. [doi: 10.1016/j.amjcard.2016.03.013]

Rubaj, A., Rucinski, P., Kutarski, A., Dabrowska-Kugacka, A., Oleszczak, K., Zimon, B., *et al.*, 2013. Cardiac hemodynamics and proinflammatory cytokines during biatrial and right atrial appendage pacing in patients with interatrial block. *Journal of Interventional Cardiac Electrophysiology*, **37**(2):147-154. [doi: 10.1007/s10840-013-9792-8]

Shou, G., Xia, L., Jiang, M., Liu, F. and Crozier, S., Year. Forward and inverse solutions of electrocardiography problem using an adaptive BEM method. International Conference on Functional Imaging and Modeling of the Heart. p. 290-299. [doi: 10.1007/978-3-540-72907-5_30]

Spodick, D.H. and Ariyarajah, V., 2010. Interatrial block: the pandemic remains poorly perceived. *Pacing & Clinical Electrophysiology*, **32**(5):667-672. [doi: 10.1111/j.1540-8159.2009.02343.x]

Tapanainen, J.M. and Jurkko, R.F., 2009. Interatrial right-to-left conduction in patients with paroxysmal atrial fibrillation. *Journal of Interventional Cardiac Electrophysiology*, **25**(2):117-122. [doi: 10.1007/s10840-008-9359-2]

Tekkesin, A.I., Çinier, G., Cakilli, Y., Hayıroğlu, M.İ. and Alper, A.T., 2017. Interatrial block predicts

atrial high rate episodes detected by cardiac implantable electronic devices. *Journal of Electrocardiology*, **50**(2):234-237. [doi: 10.1016/j.jelectrocard.2016.09.004]

Tse, G., Lai, E.T.H., Jie, M.Y. and Yan, B.P., 2016. Electrophysiological Mechanisms of Bayés Syndrome: Insights from Clinical and Mouse Studies. *Frontiers in Physiology*, **7**(188. [doi: 10.3389/fphys.2016.00188]

Tse, G., Wong, C.W., Gong, M., Wong, W.T., Bazoukis, G., Wong, S.H., *et al.*, 2017. Predictive value of inter-atrial block for new onset or recurrent atrial fibrillation: A systematic review and meta-analysis. *International Journal of Cardiology*. [doi: 10.1016/j.ijcard.2017.09.176]

Verlato, R., Botto, G.L., Massa, R., Amellone, C., Perucca, A., Bongiorni, M.G., *et al.*, 2011. Efficacy of low interatrial septum and right atrial appendage pacing for prevention of permanent atrial fibrillation in patients with sinus node disease: results from the electrophysiology-guided pacing site selection (EPASS) study. *Circ Arrhythm Electrophysiol*, **4**(6):844-850. [doi: 10.1161/CIRCEP.110.957126]

Vignendra, A.M.D., Mark, K.M.D., Sirin, A.M.D. and D.Sc, D.H.S.M.D., 2007. Potential Factors That Affect Electrocardiographic Progression of Interatrial Block. *Annals of Noninvasive Electrocardiology*, **12**(1):21-26. [doi: 10.1111/j.1542-474X.2007.00134.x]

Waldo, A.L., Jr, B.H., Gelband, H., Jr, Z.G., Vitikainen, K.J. and Hoffman, B.F., 1971. Effects on the canine P wave of discrete lesions in the specialized atrial tracts. *Circulation Research*, **29**(5):452-67. [doi: 10.1161/01.RES.29.5.452]

Wu, J.T., Wang, S.L., Chu, Y.J., Long, D.Y., Dong, J.Z., Fan, X.W., *et al.*, 2017. CHADS2 and CHA2DS2-VASc Scores Predict the Risk of Ischemic Stroke Outcome in Patients with Interatrial Block without Atrial Fibrillation. *Journal of Atherosclerosis & Thrombosis*, **24**(2):176-184. [doi: 10.5551/jat.34900]

Xia, L., Huo, M., Wei, Q., Liu, F. and Crozier, S., 2006. Electrodynamic heart model construction and ECG simulation. *Methods of Information in Medicine*, **45**(5):564-573.

Zhang, Y., Xia, L., Gong, Y., Chen, L., Hou, G. and Tang, M., Year. Parallel solution in simulation of cardiac excitation anisotropic propagation. International Conference on Functional Imaging and Modeling of the Heart. p. 170-179. [doi: 10.1007/978-3-540-72907-5_18]